Gallo, Pasquale; Bressan, Stefano; Morishita, Takahiro; Itoh, Takamoto; Berto, Filippo

Analysis of multiaxial low cycle fatigue of notched specimens for type 316L Stainless Steel under non-proportional loading

Published in:
Theoretical and Applied Fracture Mechanics

DOI:
10.1016/j.tafmec.2017.01.009

Published: 01/01/2017

Analysis of Multiaxial Low Cycle Fatigue of Notched Specimens for Type 316L Stainless Steel under Non-proportional Loading

Pasquale GALLO[1], Stefano BRESSAN[2], Takahiro MORISHITA[2], Takamoto ITOH[3,*] and Filippo BERTO[4]

[1] *Aalto University, Department of Mechanical Engineering, Marine Technology, Puumiehenkuja 5A, 02150 Espoo, Finland*
[2] *Ritsumeikan University, Graduate School of Science & Engineering, 1-1-1, Nojihigashi, Kusatsu-shi, Shiga, 5258577, Japan*
[3] *Ritsumeikan University, Department of Mechanical Engineering, College of Science & Engineering, 1-1-1, Nojihigashi, Kusatsu-shi, Shiga, 5258577, Japan*
[4] *NTNU, Department of Engineering Design and Materials, Richard Birkelands vei 2b, 7491, Trondheim, Norway*

Abstract

The paper analyzes multiaxial low cycle fatigue tests of notched specimens under proportional and non-proportional loading conditions. Strain controlled multiaxial low cycle fatigue tests were carried out using circumferentially notched round-bar specimens of Type 316L stainless steel, with different stress concentration factors. The experimental results show that the crack initiation site is shifted from the notch tip. Based on this finding, a new model for life evaluation is proposed by taking into account the strain gradient in the proximity of the notch tip and the effective maximum strain range. The new model allows evaluating the fatigue life in a narrow scatter band.

Keywords: Multiaxial fatigue; non-proportional loading; notch; 316L stainless steel.

***Corresponding author:** itohtaka@fc.ritsumei.ac.jp (T. Itoh)

Nomenclature

f_{NP}	non-proportional factor
E	elastic modulus
K'	cyclic strength coefficient
$K_{t,n}$	elastic stress concentration factors referred to the net section
K_t'	cyclic strength coefficient proposal
n'	cyclic strain hardening exponent
N_f	number of cycles to failure
r_0	distance from notch tip
α	material constant
ε_f'	fatigue ductility coefficient
$\Delta\varepsilon_{eq}$	strain range based on von Mises
$\Delta\varepsilon_I$	principal strain range
$\Delta\varepsilon_{NP}$	non-proportional strain range
$\Delta\tau_{loc}$	local shear stress range
$\Delta\tau_{max}$	maximum shear stress range
θ_a	notch opening angle
θ_p	preliminary angle within the maximum strain node and the notch tip
θ_p'	angle θ_p divided by $K_{t,n}$
R_τ	shear stress ratio
ρ	notch radius
σ'_{loc}	local stress corresponding to the maximum strain
σ_n	nominal stress referred to the net section
σ_f'	fatigue strength coefficient
$\sigma_{n,max}$	maximum stress acting normal to a plane
SWT	Smith, Watson and Topper model damage parameter
SWT'	modified SWT parameter

1. Introduction

Components and structures in several engineering applications, such as high temperature exchangers and nuclear vessels of fast breeder reactors, undergo multiaxial low cycle fatigue (LCF) under non-proportional loading in which principal stress and strain directions are changed in a cycle. Unlike the uniaxial loading condition, multiaxial fatigue presents higher grade of complexity, due to several factors, such as the complex stress states and/or loading history. For the evaluation of fatigue life of components subjected to such critical conditions, different approaches have been developed and reported in several works [1–5]. Pioneering works on the life evaluation under non-proportional loading were mainly based on critical plane approaches, such as Fatemi-Socie [6] and Smith-Watson-Topper (SWT) [7]. Other authors instead, focused on energetic approaches for the fatigue life assessment under non-proportional loadings and, more in general, under localized plastic phenomenon [8–14]. Critical plane and energy approaches found good applicability of fatigue life evaluation in multiaxial high cycle and LCF under proportional loading condition. However, components might be subjected mainly to non-proportional loading in operating conditions. This situation affects the fatigue life and hardening behavior of the component: fatigue life is usually reduced and an additional hardening occurs compared to proportional loading as reported in several references [15–17]. In general, when classical models are applied to non-proportional loading, fatigue life tends to be overestimated.

While many studies have been carried out considering multiaxial fatigue of smooth specimens, a limited number of papers have been reported for notched specimens. The evaluation of the local stresses and strains near a critical feature, such as a notch, is of primary importance for a correct and reliable estimation of the fatigue life. However, this task is far from easy. When dealing with notches, indeed, only the nominal load is known, while the local parameters are estimated involving more sophisticated methods and variables (e.g. geometry, mechanical properties, loading history) [18–20]. In case of complex geometries, the post-processing of incremental nonlinear FE models seems a reliable solution to obtain the local stress-strain histories, as shown by several authors [21,22], but it is computationally expensive and not effective in case of complex geometries. For these reasons, simpler methods are desirable, for example combining model for the local stress and strain estimation, together with material constitutive relations. When dealing with notched components, the stress concentration factor is defined considering the notch root/tip or in general the point where the maximum stress occurs. However, stress and strain gradient moving away from the tip can be present and plays a fundamental role in the fatigue failure. For this reason, the failure should be considered as taking place over a volume rather than in a point. An analysis of the variation of stress and strain in the volume surrounding the notch is always desirable, in order to avoid overly conservative life predictions [20,23,24]. Some authors, in the past and recent literature, dealt with these matters. In a reference [25] the notch effect the multiaxial LCF is investigated. The number of cycles to crack initiation was found to be significantly influenced by notch radius. Those authors also showed that the additional hardening at the notch tip plays an important role in the fatigue process.

Itoh and Sakane [26,27] proposed a strain based model which takes into account additional hardening and strain path. A new strain parameter, $\Delta\varepsilon_{NP}$, called *non-proportional strain range*, was defined to assess failure life. This model has been applied widely to hollow cylinder smooth specimens made by different materials, and its accuracy was verified comparing the results from proportional and non-proportional loadings. The results were successfully synthesized in a factor two band which suggested a good estimation of fatigue life and an accurate interpretation of the factors involved in the proposed model [28,29]. Recently, Itoh et al. [30,31] analyzed notched specimens under proportional and non-proportional LCF, and the Itoh-Sakane model for life evaluation was modified by considering local parameters of strain.

The present paper reanalyzes the experimental multiaxial LCF tests under non-proportional loading conducted by Itoh and collaborators [30] with additional experimental tests, on Type 316L stainless steel (SUS316L) notched specimens. A modified Itoh-Sakane's model is proposed, taking into account the gradient effect by the definition of a new stress concentration factor shifted from the point at notch tip. The new model allows evaluating the fatigue life in a narrow scatter band. The model is well supported by original finite element analyses that consider the cyclic stress and strain curves obtained experimentally. In detail, the specimen was modeled in different areas with different hardening levels. By using this technique, the analysis of the hardening behavior is heavily simplified but reliable approximation of plasticity effect is taken into account for the specific case studied here.

The paper is motivated by the fact that a deviation from the notch tip of the crack initiation point was detected experimentally for some specimens, due to the steep strain gradient at the notch tip. The analysis permitted the evaluation of local parameters, such as stresses and strains, that allowed the authors to better understand the local hardening behavior and to develop the improvement of their original model [26,27]. Comparison of the obtained results with Smith-Watson-Topper approach [7] is also presented.

2. Non-proportional Multiaxial Fatigue Tests

Non-proportional multiaxial fatigue tests were carried out by a circumferentially notched round-bar specimen made of AISI316L. The specimens are provided in annealed condition (solution heat treatment at 1353 K). Different stress concentration factors $K_{t,n}$ =1.5, 2.5, 4.2 and 6.0 were employed. Geometrical specifications are depicted in Fig. 1 (a)-(d).

The specimens were tested by using proportional and non-proportional strain paths. Proportional load is represented both by push-pull loading (push-pull) and reversed torsion loading (rev. torsion) tests. Non-proportional load is represented by a circle loading (circle) test in which equivalent stress and strain assumes the same value for all the duration of the cycle, as shown in Fig. 2. Cyclic stress and strain curves were obtained from a step up test where strain range was increased by 0.1% every 10 cycles. As shown in Fig. 3, the curve of the circle test is higher than that of the push-pull test due to the additional hardening of non-proportional loading.

Tests were made by applying a von Mises equivalent and constant strain range $\Delta\varepsilon_{eq}$, equal to 0.7%. Axial and shear displacements were measured through an extensometer, and gage length was 7 mm for all the specimens. The number of cycles to failure N_f, is defined as the number of cycles at which the stress amplitude becomes 3/4 of the maximum value. The detailed results are summarized in Table 1. Non-proportional and additional hardening effects on fatigue life are very clear, the fatigue life of non-proportional loading tests is lower than proportional one comparing the results from the same stress concentration factor.

From a detailed analysis of the tested specimens, the crack initiation was detected shifted from the notch tip where the largest concentration of stress occurs. This assertion is clearly depicted in Fig. 4. This behavior is mainly due to local hardening caused by non-proportional loading, and suggests that another quantity, different from the concentrated stress due to the notch tip, controlled the failure of the specimens. Indeed, when dealing with notches, usually a steep stress or strain gradient moving away from the notch tip exists. The gradient plays an important role in the fatigue failure of the component, and should be accurately considered, taking into account a volume zone rather than the point where the maximum stress occurs.

In addition to the analysis of the crack initiation zone, further analyses were carried out on the hardness evolution during the tests. In detail, the hardness was detected on 5 directions (0°, 10°, 30°, 50° and 70°) along the longitudinal section of the specimens after $0.3N_f$ (see Fig. 5). The detected hardness is shown in Fig. 6 (a) and (b) along 0° direction that corresponds to the notch bisector. Maximum value of hardness in notched specimens depends both on strain paths and notch tip radius, confirming that non-proportional loading has a great influence on additional hardening. Based on the hardness values of the spots evidenced in Fig. 5, an approximated hardness distribution is obtained and reported in Fig. 7. Even if the hardness maps of Fig. 7 might not reflect accurately the continuous and gradual real variation of the hardness, they are a useful approximation to show the distribution of hardness around the notch tip, depending on $K_{t,n}$ and strain path.

3. Itoh-Sakane Model for Fatigue Life Evaluation under Non-proportional Loading

Itoh-Sakane (IS) model was originally developed for fatigue assessment of smooth specimen made of different materials subjected to proportional and non-proportional loadings [26,27]. The model introduced two factors for the evaluation of the failure life: the non-proportional factor f_{NP} which expresses the intensity of non-proportional loading, and the material constant α which is related to the material additional hardening due to non-proportional loading. By these factors, a strain parameter, $\Delta\varepsilon_{NP}$ is derived, starting from the experimental principal strain range $\Delta\varepsilon_I$,

$$\Delta\varepsilon_{NP} = \left(1+\alpha f_{NP}\right)\Delta\varepsilon_I \tag{1}$$

Equation 1 represents the Itoh-Sakane model in its damage parameter. The explicit formulation of the model that correlates $\Delta\varepsilon_{NP}$ and the number of cycle to failure is reported for the sake of clarity in Eq. (2)

$$\Delta\varepsilon_{NP} = \frac{3.5\sigma'_f}{E} N_f^{-0.12} + \varepsilon_f'^{0.6} N_f^{0.6} \tag{2}$$

where E, σ_f' and ε_f' are Yong's modulus, a tensile strength and an elongation, respectively. In this study, E and σ_f' are put as the mechanical properties obtained from the tensile test but ε_f' is defined to fit the fatigue life curve to the data of the push-pull loading test.

For the AISI316L the constant α takes the value of 0.9. The non-proportional factor, f_{NP}, takes the value of 1 for the circle condition and 0 for the push-pull and the rev. torsion condition. The model can be applied to smooth specimens since $\Delta\varepsilon_I$ corresponds to the maximum nominal strain range. Similarities with critical plane approaches can be observed. However, the IS's model simplifies the estimation of the fatigue life by modifying the maximum strain range parameter, without the necessity of detecting the critical plane as a first step. This point is better discussed later in the paper. In Eq. (1), $\Delta\varepsilon_I$ can be replaced by such as an equivalent strain range of Von Mises or Tresca.

Since many components have complex shapes, stress concentration effects may occur. In these cases $\Delta\varepsilon_I$ does not correspond anymore to the maximum strain and $\Delta\varepsilon_{NP}$ should be evaluated starting from local strain values. The authors tried to apply the relationship between $\Delta\varepsilon_{NP}$ and N_f to notched specimens, evaluating the local stress by $K_{t,n}$ and assuming the corresponding local strain at the notch tip,

$$K_{t,n}\,\Delta\varepsilon_{NP} = K_{t,n}\left(1+\alpha f_{NP}\right)\Delta\varepsilon_{I} \tag{3}$$

Results of the application of this model are summarized in Fig. 8. A factor of 2 band represents the data of hollow cylinder smooth specimens obtained in a previous work [28]. Non-proportional strain range is well correlated with N_f even for notched specimens with different notch severity. Since $K_{t,n}$ is evaluated under linear elastic condition, its employment under LCF, when plastic deformations occur severely, introduces unavoidable approximations. To consider plastic deformations, Neuber's rule [32] can be applied to evaluate local strain, with an overestimation of the fatigue life [25]. Alternatively, finite element analysis is employed to evaluate the local parameters, as shown in previous works [25,30] but with high computational cost.

Data presented in [28,30] is also analyzed by means of SWT approach shown in Eq. (4) for comparison,

$$\mathrm{SWT} = \sigma_{n,\max}\,\frac{\Delta\varepsilon_{I}}{2} \tag{4}$$

where $\Delta\varepsilon_I$ is the principal strain range, and $\sigma_{n,\max}$ is the maximum stress on the principal strain range plane. Effects of non-proportional loading are included in the $\sigma_{n,\max}$, and the SWT parameter does not need any additional modifications. When dealing with notched specimens, the stress concentration factor is introduced and Eq. (4) becomes,

$$\mathrm{SWT} = K_{t,n}\,\sigma_{n,\max}\,\frac{\Delta\varepsilon_{I}}{2} \tag{5}$$

The results are reported in Fig. 9. As shown in the figure, SWT returns a slightly larger scatter band of 2.5, comparing with the IS model of Fig. 8 where the scatter band is of a factor of 2.0.

4. Evaluation of Local Parameters by Finite Element Modeling

4.1 Modeling procedure

As mentioned above, the application of IS's model relies on the knowledge of local parameters. These are evaluated on the basis of liner elastic behavior neglecting the plastic contribution, or with a finite element analysis in order to take into account the effects of inelastic deformation and hardening occurring at the notch tip. As shown in Fig. 7, it emerges that the hardening occurred around the notch tip is not uniform, but different zones with different levels of hardening are observed. In order to faithfully replicate this behavior in numerical simulations, a particular technique is employed. The notch tip is divided in different hardening areas and a cyclic stress and strain curve is assigned to each area. Even if a simplification, circular areas were modeled. The minimum and maximum hardness are represented by the cyclic stress and strain curves in the push-pull and the circle experimental test, respectively. For this reason, the cyclic stress and strain curve in the push-pull test was assigned to the material close to the axis of symmetry, far from the notch tip, while the cyclic stress and strain curve in the circle test to the outer surface of the notch tip. This assumption is supported by the hardness maps obtained experimentally which show a gradually decrement of the hardness moving away from the notch tip. The same hypothesis can be drawn by simple considerations based on the shear stress. As shown in Fig. 10, the shear stress assumes maximum value at the outer surface that corresponds to the circle condition. However the shear stress becomes zero at axis of the specimen, and the push-pull condition can be assumed. Through best fitting and extrapolation procedures, intermediate cyclic stress and strain curves to be assigned to the intermediate circular areas are estimated and modeled following the variation of shear stress ratio R_τ, where R_τ is evaluated as the ratio within local shear stress range $\Delta\tau_{loc}$ and maximum shear stress range $\Delta\tau_{max}$ by,

$$R_\tau = \frac{\Delta\tau_{loc}}{\Delta\tau_{max}} \tag{6}$$

The circle condition was related to 100% of R_τ while the push-pull condition to 0%.

The procedure followed for the determination of the intermediate cyclic stress and strain curves is presented exhaustively later. By using this modeling technique, the cyclic hardening behavior was intrinsically taken into account. A static axial loading corresponding to the maximum axial nominal stress range recorded in experimental tests (see Table 1) was applied. As a final result, values and positions of local strain and stresses were obtained.

4.2 Modeling of the notch tip hardening behavior

The following power law constitutive equation was employed to describe the cyclic non-linear relationship between the stress and plastic strain,

$$\Delta\sigma = K'\Delta\varepsilon^{n'} \tag{7}$$

The cyclic strength coefficient K' and the cyclic strain hardening exponent n' were obtained by best fitting of the plastic trend of the cyclic stress and strain curves in the push-pull and circle tests as shown in Fig. 3,

$$\Delta\sigma = 1502\ \Delta\varepsilon^{0.2756} \qquad \text{push-pull} \tag{8}$$

$$\Delta\sigma = 11210\ \Delta\varepsilon^{0.5893} \qquad \text{circle} \tag{9}$$

Equation (8) was assigned to the material close to the axis of symmetry far from the notch tip (push-pull), Eq. (9) at the outer surface of the notch tip, respectively (circle condition). The intermediate cyclic stress and strain curves to be assigned to the intermediate circular areas were instead estimated and modeled following the variation of shear stress in percentage value. By modifying K' and n' parameters, the intermediate cyclic stress and strain curves were obtained. In order to obtain a high grade of optimization and automation of the intermediate cyclic stress and strain curves generation as a function of the shear stress, the following equations were developed,

$$K' = 1510\ e^{0.0198\,R_\tau} \tag{10}$$

$$n' = 0.0031\ R_\tau + 0.2754 \tag{11}$$

Equations (10) and (11) permit to obtain an arbitrary number of cyclic stress and strain curves, as a function of the modeled areas and of the shear stress distribution. These are included within the cyclic stress and strain curves of the push-pull and circle loading conditions. It is evident from the formulation of the last Eqs. (10) and (11), that the parameter K' was assumed to vary according to exponential law, while the parameter n' has a linear trend. Figures 11 and 12 show examples of the trend of the hardening parameters as a function of the shear stress variation. Figure 13 depicts an example of the cyclic stress and strain curves obtained varying hardening parameters according to Eqs. (10) and (11). In the present paper, 100 areas are assumed as a good trade off within accurate results and computational cost. As a consequence, 100 cyclic stress and strain curves are modeled to describe the notch-tip hardening behavior. The linear elastic trend was maintained constant following the mechanical properties reported in [30] that are E=197 GPa and ν=0.3.

4.3 Finite element modeling

An accurate 2D finite element model of the notched specimens was realized through APDL ANSYS FE tool. The high order element SOLID273 was employed assuming axisymmetric key option, and a fine mesh was realized. The multilinear isotropic hardening model (MISO) was assumed to describe the elastic-plastic behavior of the component. In total, 100 cyclic stress and strain curves were modeled and assigned to the 100 circular areas in which the notch tip was divided. Each area represents an increment of the shear stress equal to 1%. Figure 14 depicts the model and the circular areas around the notch tip for the specimen represented in Fig. 1a ($K_{t,n}$=1.5).

The dimension and position of the areas were selected based on the shear stress variation that depends on $K_{\mathrm{t,n}}$. Figure 15 shows the trends of the shear stress variation as a function of $K_{\mathrm{t,n}}$ and distance from the notch tip applying a pure torsion load to the specimen. Smaller areas, relatively close to each other, were modeled for high variations of the shear stress, while bigger areas relatively far from each other for small variations. The final results is depicted in Fig. 16, considering the specimen of Fig. 1a ($K_{\mathrm{t,n}}$=1.5).

Mesh convergence study was performed until the results were stable and not affected by the mesh refinement.

5. Results and Discussion

Local stresses and strains were obtained through the finite element simulation presented previously and permitted to investigate the gradient occurring around the notch tip. The contour plots of Fig. 17 show that the positions of the maximum strain and of the notch root (where one obtains the maximum stress) are different. This phenomenon is verified for all of the considered geometries. For the sake of brevity, only the results regarding $K_{\mathrm{t,n}}$=1.5 and 4.2 are reported in Fig. 17. The location of the maximum strain corresponds to the shifted crack initiation site detected from experimental results (see Fig. 4). This deviation from the notch tip is quantified in terms of angle and summarized in Table 2. A reference center is defined at distance from the notch tip $r_0 = \rho(\pi - 2\alpha)/(2\pi - 2\alpha)$ (ρ is the notch radius while 2α is the notch opening angle) in according with auxiliary system of curvilinear coordinates defined by Neuber [33] and other authors when dealing with notches [34–39]. Once defined the center, a preliminary angle θ_p within the maximum strain node and the notch tip is evaluated. To take into account the different notch radius, θ_p was divided by the stress intensity factor $K_{\mathrm{t,n}}$, obtaining the final results θ_p' reported in Table 2. This expedient takes into account the different sharpness of the notches and permits a correct comparison within different geometries. Figure 18 depicts the center and the angle for the sake of clarity.

The obtained new local parameters is employed in the IS's model. In details, a new stress concentration factor K_t' is evaluated as the ratio within the stress σ'_{loc} corresponding to the maximum strain and nominal stress σ_n referred to the net section,

$$K' = \frac{\sigma'_{loc}}{\sigma_n} \tag{12}$$

K_t' is used in substitution of the common stress concentration factor, referred to elastic conditions. The new IS's model formulation becomes,

$$K_t' \, \Delta\varepsilon_{NP} = K_t' \left(1 + \alpha \, f_{NP}\right) \Delta\varepsilon_I \tag{13}$$

Table 2 reports the values of the K_t' and elastic $K_{t,n}$ for the considered geometries. The experimental data presented in the previous section is reanalyzed by mean of Eq. (13). The new results, compared with the one previously obtained by the present authors [30], are shown in Fig. 19. The new formulation permits to summarize the results in a narrow scatter band and it takes into account the real behavior of the component. The original data, in fact, was synthesized in a factor of 2 band, while using the new formulation a new factor 1.6 band is obtained. The local parameters based on the proposed formulation consider strain and stress values at the real crack initiation point. This interpretation allows the IS's model to consider the faithful damage processing. The employment of the linear elastic $K_{t,n}$, despite a sufficient correlation of the results, did not take into account the real damage processing. The existence of a shifted maximum strain was supposed by the author on the basis of past results, but it was not investigated in detail [25,30]. According to the analysis carried out in the present paper, the real local parameter is evaluated and employed, resulting in an improvement of the original results.

The results are also additionally compared with the one obtained by a modified SWT approach, in which the shifted K_t' is employed instead of the common stress concentration factor. The modified SWT parameter becomes,

$$\mathrm{SWT}' = K'_t \, \sigma_{n,max} \frac{\Delta\varepsilon_I}{2} \tag{14}$$

The results are shown in Fig. 20, together with the original scatter band. From the results, it is clear that if modified stress concentration factor is employed in the SWT formulation, the original scatter band of 2.5 increases and becomes equal to 4.

The evaluation of fatigue life through the IS's model, unlike the SWT approach, is not related to the definition of the critical plane. This solution simplifies the evaluation of the multiaxial fatigue life since in some cases the detection of the critical plane is complex. On the other hand, this simplification involves also limitations when IS's model is applied to non-proportional loads combined with complex loading history such as random loading. In this case, in fact, the plane of maximum strain range usually does not coincide with the plane where the fracture occurs. In addition, the model can be applied only to tensile-sensitive material, where the cracks tend to initiate on critical planes defined by normal/principal components. In the present paper, the model has been applied to the tensile-sensitive material AISI316L and only simple cyclic loads have been considered. Under these conditions, the critical plane is defined by the principal components of the load cycle, and the IS's model gives comparable or even better results (when modified stress concentration factor is employed) than the SWT approach.

The limitations of the IS's model described above have been also considered in developing the finite element analyses procedure described in Section 4. The method, in fact, is an approximation for simple periodic non-proportional loading, since the material behavior changes in space (several areas with different hardening behavior have been modeled) but not in the time domain. Despite this, the procedure is valid because applied to a specific case in which simple loads are considered. Moreover, it has been developed in order to obtain the parameters needed in the IS's model. Random or in general not simple periodic non-proportional loading would need the application of more sophisticated incremental plasticity calculations, as well as the application of different fatigue models.

6. Conclusions

The present work outlines a new formulation and improvement of the Itoh-Sakane's model for multiaxial fatigue under non-proportional loading of notched components. On the basis of accurate finite element analyses, new local parameters are evaluated and employed in the original formulation. In detail, the model is divided in several areas to which a specific cyclic stress and strain curve is assigned, in order to reproduce the local hardening. This approach permits to obtain a model with a progressive transition within the pure push-pull behavior occurring at the axis of symmetry (null shear stress) to the circle test at the notch tip (maximum shear stress). A simple tensile load test is subsequently applied since hardening effect was intrinsically considered in the modeling.

The main conclusions can be summarized as follow;

1. The analyses show that the maximum strain does not occur at the notch tip but it is shifted from that position as a function of the stress concentration factor and so of the geometry. This behavior becomes more evident for lower $K_{t,n}$. For higher $K_{t,n}$, because of the high stress concentration effect, the displacement from the notch tip tends to be lower.
2. The shifted maximum strain justifies the experimental evidence emerged from previous work [30]. The crack initiation site was not located at the notch tip, where the maximum stress occurs, but where the maximum strain occurs.
3. A new K_t' is defined as the ratio within the stress occurring at the maximum strain and the nominal net stress, and employed in the Itoh-Sakane's model. A narrower scatter band is obtained, compared to the original results.
4. The model gives a simplified procedure for LCF simulation: a simple tensile static simulation returns very good results and the cyclic hardening behavior is intrinsically considered. These procedure, however, is limited to simple periodic non-proportional loadings and in combination with the IS's model.
5. Despite some limitations, the proposed modeling procedure is particularly useful in such cases when the parameters for cyclic simulation modeling are not available.

Acknowledgement

Part of this work was supported by JSPS KAKENHI Grant Number JP15K05698 and KOKUSAITEKI Research Fund in Ritsumeikan University (Research Fund for Promoting International Research Activities in the Doctoral Degree Program).

References

[1] Y. Liu, S. Mahadevan, Multiaxial high-cycle fatigue criterion and life prediction for metals, Int. J. Fatigue. 27 (2005) 790–800. doi:10.1016/j.ijfatigue.2005.01.003.

[2] Y. Garud, Multiaxial Fatigue: A Survey of the State of the Art, J. Test. Eval. 9 (1981) 165–178.

[3] Y. Wang, Evaluation and comparison of several multiaxial fatigue criteria, Int. J. Fatigue. 26 (2004) 17–25. doi:10.1016/S0142-1123(03)00110-5.

[4] B. You, A critical review on multiaxial fatigue assessments of metals, Int. J. Fatigue. 18 (1996) 235–244. doi:10.1016/0142-1123(96)00002-3.

[5] A. Fatemi, N. Shamsaei, Multiaxial fatigue: An overview and some approximation models

for life estimation, Int. J. Fatigue. 33 (2011) 948–958. doi:10.1016/j.ijfatigue.2011.01.003.

[6] A. Fatemi, D.F. Socie, A critical plane approach to multiaxial fatigue damage inlcunding out-of-phase loading, Fatigue Fract. Eng. Mater. Struct. 11 (1988) 149–165. doi:10.1111/j.1460-2695.1988.tb01169.x.

[7] K.N. Smith, P. Watson, T.H. Topper, Stress-strain function for fatigue of metals, J. Mater. 5 (1970) 767–778.

[8] P. Gallo, F. Berto, G. Glinka, Generalized approach to estimation of strains and stresses at blunt V-notches under non-localized creep, Fatigue Fract. Eng. Mater. Struct. 39 (2016) 292–306. doi:10.1111/ffe.12374.

[9] P. Gallo, F. Berto, Advanced Materials for Applications at High Temperature: Fatigue Assessment by Means of Local Strain Energy Density, Adv. Eng. Mater. (2015) n/a-n/a. doi:10.1002/adem.201500547.

[10] F. Berto, P. Gallo, Extension of linear elastic strain energy density approach to high temperature fatigue and a synthesis of Cu-Be alloy experimental tests, Eng. Solid Mech. 3 (2015) 111–116. doi:10.5267/j.esm.2015.1.004.

[11] A. Moftakhar, A. Buczynski, G. Glinka, Calculation of elasto-plastic strains and stresses in notches under multiaxial loading, Int. J. Fract. 70 (1995) 357–373. doi:10.1007/BF00032453.

[12] A. Moftakhar, G. Glinka, D. Scarth, D. Kawa, Multiaxial stress-strain creep analysis for notches, in: ASTM Spec. Tech. Publ., ASTM, 1994: pp. 230–243.

[13] F. Berto, A. Campagnolo, P. Gallo, Brittle Failure of Graphite Weakened by V-Notches: A Review of Some Recent Results Under Different Loading Modes, Strength Mater. 47 (2015) 488–506. doi:10.1007/s11223-015-9682-7.

[14] R. Negru, S. Muntean, N. Pasca, L. Marsavina, Failure assessment of the shaft of a pumped storage unit, Fatigue Fract. Eng. Mater. Struct. 37 (2014) 807–820. doi:10.1111/ffe.12187.

[15] D.F. Socie, Multiaxial Fatigue Damage Models, J. Eng. Mater. Technol. 109 (1987) 293–298. doi:10.1115/1.3225980.

[16] G. Rasheda, R. Ghajar, G. Farrahi, Multiaxial stress-strain modeling and effect of additional hardening due to nonproportional loading, J. Mech. Sci. Technol. 21 (2007) 1153–1161. doi:10.1007/BF03179030.

[17] M. Sakane, T. Itoh, T. Susaki, Y. Kawazoe, Life Prediction for Notched Components in Nonproportional Low Cycle Fatigue: Experiment and FEM Analysis, in: Press. Vessel Pip. Codes Stand., ASME, 2004: pp. 31–38. doi:10.1115/PVP2004-2670.

[18] M.E. Barkey, D.F. Socie, K.J. Hsia, A Yield Surface Approach to the Estimation of Notch Strains for Proportional and Nonproportional Cyclic Loading, J. Eng. Mater. Technol. 116

(1994) 173. doi:10.1115/1.2904269.

[19] V.B. Köttgen, M.E. Barkey, D.F. Socie, Pseudo stress and pseudo strain based approaches to multiaxial notch analysis, Fatigue Fract. Eng. Mater. Struct. 18 (2007) 981–1006. doi:10.1111/j.1460-2695.1995.tb00922.x.

[20] N. Gates, A. Fatemi, Notch deformation and stress gradient effects in multiaxial fatigue, Theor. Appl. Fract. Mech. 84 (2016) 3–25. doi:10.1016/j.tafmec.2016.02.005.

[21] M.-C. Yip, Y.-M. Jen, Mean Strain Effect on Crack Initiation Lives for Notched Specimens Under Biaxial Nonproportional Loading Paths, J. Eng. Mater. Technol. 119 (1997) 104. doi:10.1115/1.2805962.

[22] A. Savaidis, G. Savaidis, C. Zhang, Elastic–plastic FE analysis of a notched shaft under multiaxial nonproportional synchronous cyclic loading, Theor. Appl. Fract. Mech. 36 (2001) 87–97. doi:10.1016/S0167-8442(01)00059-3.

[23] T.H. Topper, R.M. Wetzel, J. Morrow, Neuber's rule applied to fatigue of notched specimens, J. Mater. JMSLA. 4 (1969) 200–209.

[24] S.M. Tripton, D. V. Nelson, Advances in multiaxial fatigue life prediction for components with stress concentrations, Int. J. Fatigue. 19 (1997) 503–515. doi:10.1016/S0142-1123(96)00070-9.

[25] M. Sakane, S. Zhang, T. Kim, Notch effect on multiaxial low cycle fatigue, Int. J. Fatigue. 33 (2011) 959–968. doi:10.1016/j.ijfatigue.2011.01.011.

[26] T. Itoh, T. Nakata, M. Sakane, M. Ohnami, Nonproportional Low Cycle Fatigue of 6061 Aluminum Alloy Under 14 Strain Paths, in: Macha Al., Ed. Multiaxial Fatigue Fract., 1999: pp. 41–54. doi:10.1016/S1566-1369(99)80006-5.

[27] T. Itoh, M. Sakane, M. Ohnami, D.F. Socie, Nonproportional Low Cycle Fatigue Criterion for Type 304 Stainless Steel, J. Eng. Mater. Technol. 117 (1995) 285. doi:10.1115/1.2804541.

[28] T. Itoh, T. Yang, Material dependence of multiaxial low cycle fatigue lives under non-proportional loading, Int. J. Fatigue. 33 (2011) 1025–1031. doi:10.1016/j.ijfatigue.2010.12.001.

[29] T. Itoh, M. Sakane, T. Morishita, Evaluation and visualization of multiaxial stress and strain states under non-proportional loading, Frat. Ed Integrità Strutt. 33 (2015) 289–301.

[30] T. Itoh, W. Chen, R. Yamamoto, Multiaxial Low Cycle Fatigue Life of Notched Specimen for Type 316L Stainless Steel under Non-Proportional Loading, J. Solid Mech. Mater. Eng. 5 (2011) 230–241. doi:10.1299/jmmp.5.230.

[31] T. Morishita, T. Itoh, Evaluation of multiaxial low cycle fatigue life for type 316L stainless

steel notched specimen under non-proportional loading, Theor. Appl. Fract. Mech. (2016). doi:10.1016/j.tafmec.2016.02.007.

[32] H. Neuber, Theory of Stress Concentration for Shear-Strained Prismatical Bodies With Arbitrary Nonlinear Stress-Strain Law, J. Appl. Mech. 28 (1961) 544. doi:10.1115/1.3641780.

[33] H. Neuber, Theory of Notch Stresses: Principles for Exact Calculation of Strength with Reference to Structural form and Material, 2nd ed., Springer-Verlag, Berlin, 1958.

[34] N.I. Muskhelishvili, Some Basic Problems of the Mathematical Theory of Elasticity, Leyden, 1953.

[35] P. Lazzarin, R. Tovo, A unified approach to the evaluation of linear elastic stress fields in the neighborhood of cracks and notches, Int. J. Fract. 78 (1996) 3–19. http://link.springer.com/article/10.1007/BF00018497 (accessed October 15, 2014).

[36] P. Gallo, F. Berto, G. Glinka, Analysis of creep stresses and strains around sharp and blunt V-notches, Theor. Appl. Fract. Mech. 85 (2016) 435–446. doi:10.1016/j.tafmec.2016.06.003.

[37] P. Gallo, T. Sumigawa, T. Kitamura, F. Berto, Evaluation of the strain energy density control volume for a nanoscale singular stress field, Fatigue Fract. Eng. Mater. Struct. 39 (2016) 1557–1564. doi:10.1111/ffe.12468.

[38] P. Gallo, F. Berto, Some considerations on the J-Integral under elastic-plastic conditions for materials obeying a Ramberg-Osgood law, Phys. Mesomech. 18 (2015) 298–306. doi:10.1134/S1029959915040037.

[39] P. Gallo, F. Berto, Influence of surface roughness on high temperature fatigue strength and cracks initiation in 40CrMoV13.9 notched components, Theor. Appl. Fract. Mech. 80 (2015) 226–234. doi:10.1016/j.tafmec.2015.07.003.

Captions

[Tables]

Table 1 Experimental results; number of cycles to failure N_f and applied strain range $\Delta\sigma$.

Table 2 Displacements within the maximum strain node and notch tip and K_t' values in the circle tests.

[Figures]

Fig. 1 Shape and dimensions of tested specimens: (a) $K_{t,n}$=1.5, (b) $K_{t,n}$=2.5, (c) $K_{t,n}$=4.2 and (d) $K_{t,n}$=6.0.

Fig. 2 Strain paths employed in the experiment.

Fig. 3 Cyclic stress and strain curves for push-pull and circle tests.

Fig. 4 Observation of fracture at notch tip.

Fig. 5 Analyzed area for hardness test and evaluation spots around the notch tip.

Fig. 6 Detected hardness along 0° direction: (a) Push-pull test and (b) Circle test.

Fig. 7 Hardness maps obtained by hardness test around the notch tip.

Fig. 8 Relationships between $K_{t,n}\,\Delta\varepsilon_{NP}$ and N_f for push-pull, rev. torsion and circle tests.

Fig. 9 Relationships between SWT and N_f for push-pull, rev. torsion and circle tests.

Fig. 10 Schematic showing of stress waveform at the axis and outer surface in circle test: shear stress is maximum at the outer surface and null at the axis.

Fig. 11 K' variation between push-pull and circle curves.

Fig. 12 n' linear trend between push-pull and circle curves.

Fig. 13 Cyclic stress and strain curves obtained as a function of K' and n'.

Fig. 14 Finite element model for $K_{t,n}$=1.5 (specimen (a) of Fig. 1): (a) 3-dimensional model and (b) Detail of the notch tip areas partition.

Fig. 15 Shear stress variation for different $K_{t,n}$ along the notch bisector.

Fig. 16 Specimen modeled with different stress and strain curves as a function of different shear stress values, $K_{t,n}$=1.5 (specimen (a) of Fig. 1).

Fig. 17 Contour plots of strain near the notch: (a) $K_{t,n}$=1.5 and (b) $K_{t,n}$=4.2.

Fig. 18 Evaluation of the angles within the maximum strain node and the notch tip; ρ is the notch radius, 2α is the notch opening angle, distance r_0.

Fig. 19 Correlation of N_f with $K_{t,n}\,\Delta\varepsilon_{NP}$ and $K_t'\,\Delta\varepsilon_{NP}$.

Fig. 20 Relationship between the modified SWT' parameter and N_f for push-pull, rev. torsion and circle tests.

Table 1

Strain path	$K_{t,n}$	$\Delta\sigma$ at 1/2 N_f (MPa)	$\Delta\sqrt{3}\tau$ at 1/2 N_f (MPa)	N_f (cycles)
Push-pull	1.5	800	—	2237
	2.5	800	—	871
	4.2	810	—	571
	6.0	830	—	418
Rev. torsion	1.5	—	720	54809
	2.5	—	910	4806
	4.2	—	890	3094
	6.0	—	850	2243
Circle	1.5	850	1030	2248
	2.5	880	1080	475
	4.2	900	1140	212
	6.0	850	930	156

Table 2

$K_{t,n}$	Displacements within the maximum strain node and notch tip					K_t'
	ρ (mm)	θ_a (deg.)	r_0 (mm)	θ_p (deg.)	θ_p' (deg.)	
1.5	3.4	49	1.44	29.3	19.5	1.2
2.5	0.8	60	0.32	37.4	14.9	1.8
4.2	0.2	60	0.08	53.4	12.7	2.8
6.0	0.09	60	0.036	57.6	9.60	4.0

Fig. 1

a

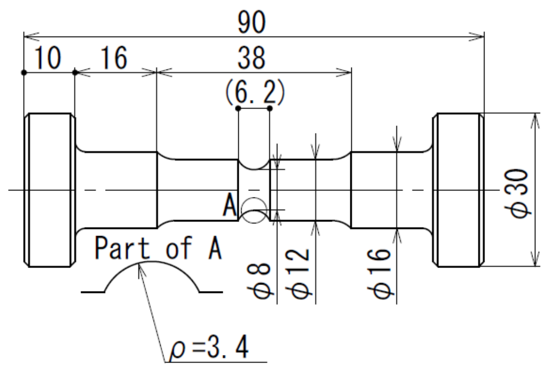
90
10
16
38
(6.2)
A
Part of A
ρ=3.4
φ8
φ12
φ16
φ30

b

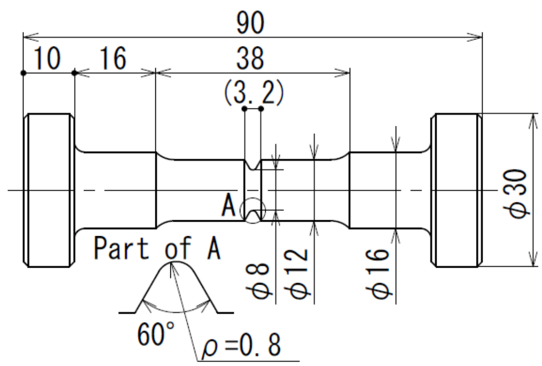
90
10
16
38
(3.2)
A
Part of A
60°
ρ=0.8
φ8
φ12
φ16
φ30

c

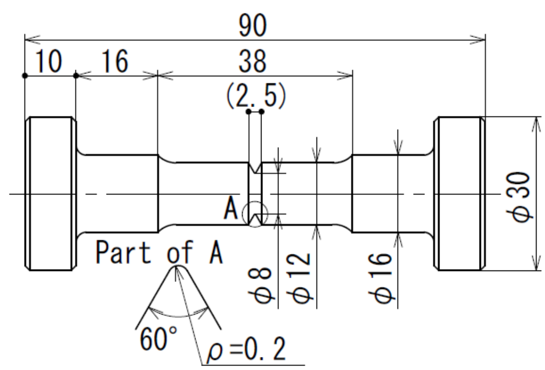
90
10
16
38
(2.5)
A
Part of A
60°
ρ=0.2
φ8
φ12
φ16
φ30

d

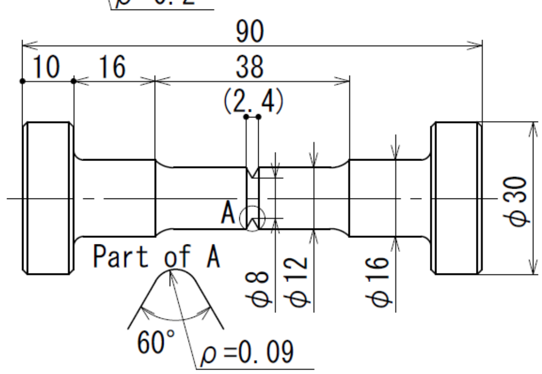
90
10
16
38
(2.4)
A
Part of A
60°
ρ=0.09
φ8
φ12
φ16
φ30

Fig. 2

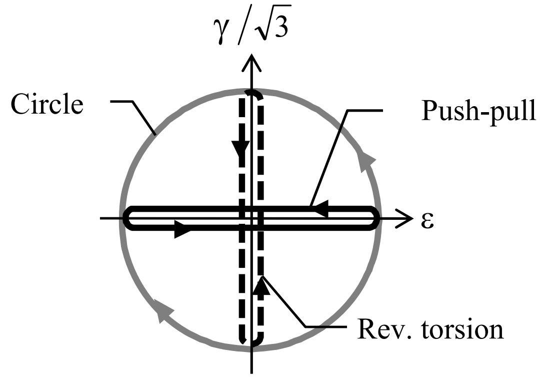

Fig. 3

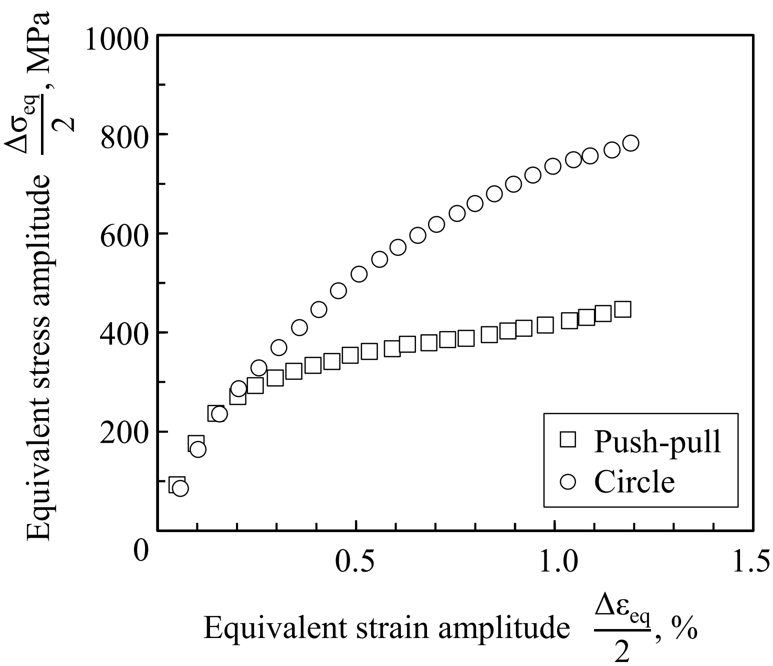
1000
800
600
400
200
0
0.5
1.0
1.5
Equivalent stress amplitude $\frac{\Delta\sigma_{eq}}{2}$, MPa
Equivalent strain amplitude $\frac{\Delta\varepsilon_{eq}}{2}$, %
Push-pull
Circle

Fig. 4

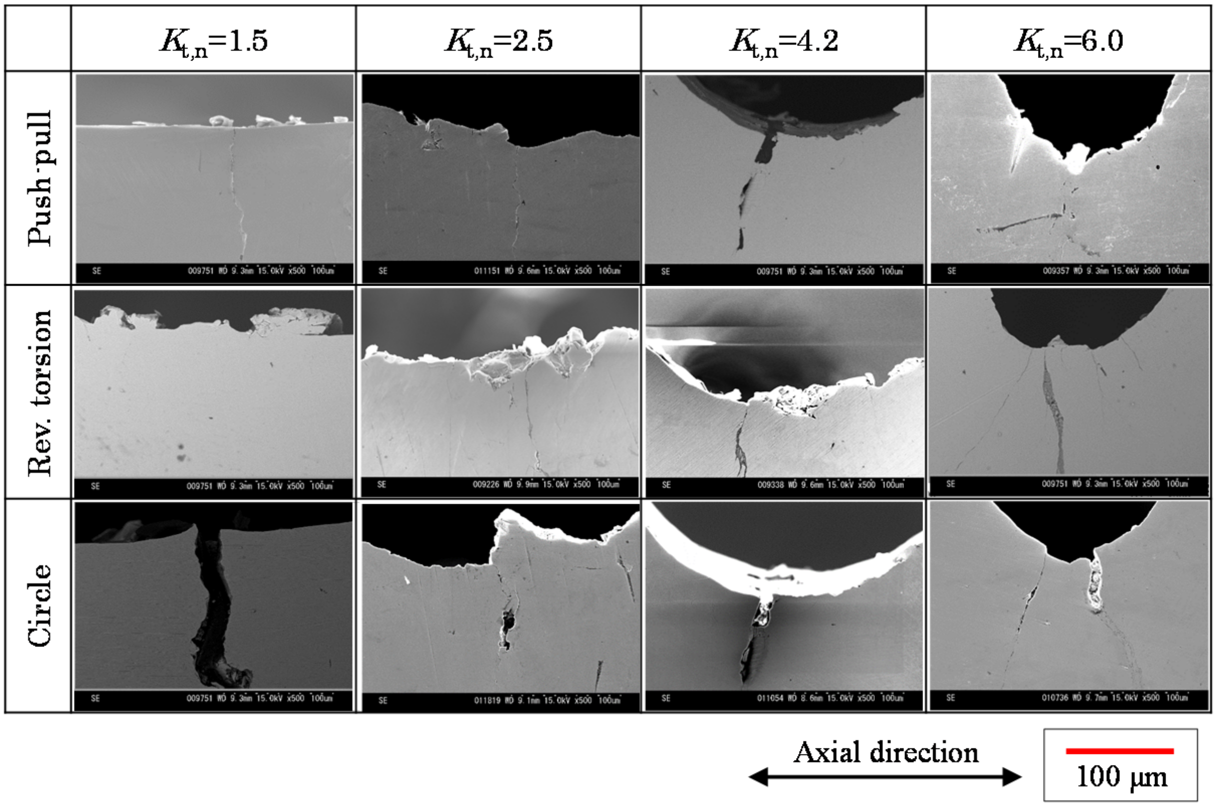

$K_{t,n}$=1.5
$K_{t,n}$=2.5
$K_{t,n}$=4.2
$K_{t,n}$=6.0
Push-pull
Rev. torsion
Circle
Axial direction
100 μm

Fig. 5

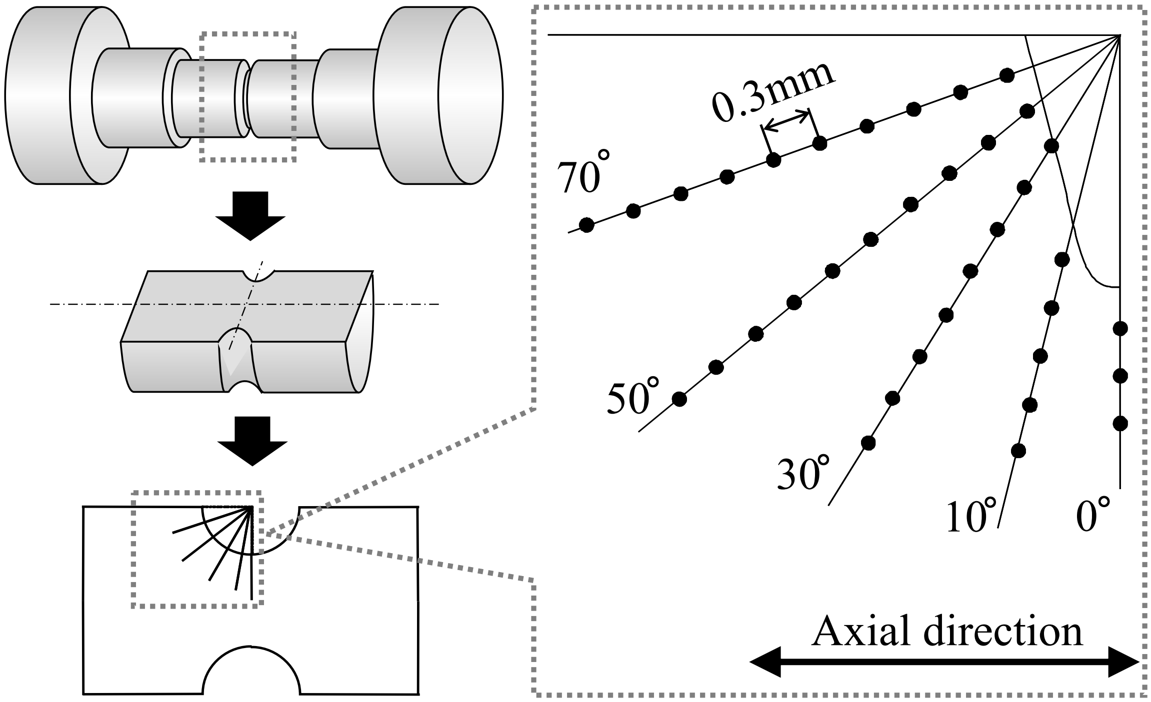

Fig. 6

a

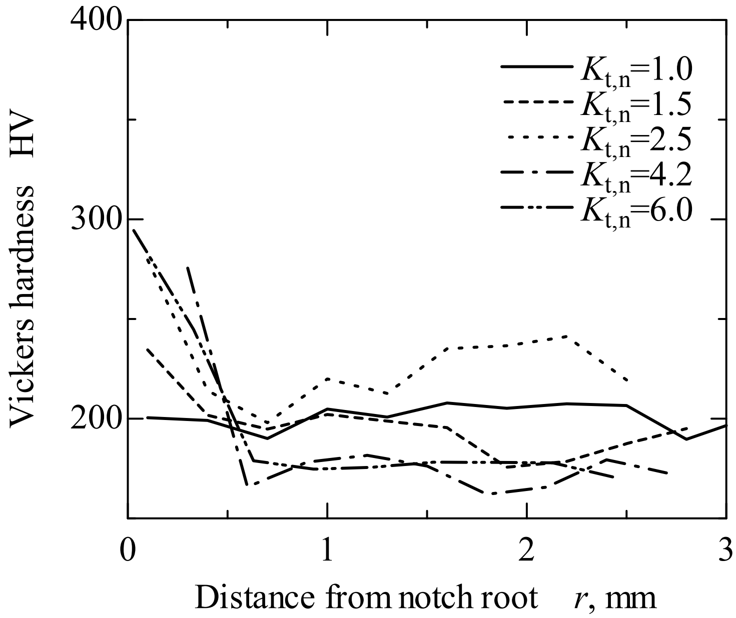

400
300
200
0
1
2
3
Vickers hardness HV
Distance from notch root r, mm
$K_{t,n}$=1.0
$K_{t,n}$=1.5
$K_{t,n}$=2.5
$K_{t,n}$=4.2
$K_{t,n}$=6.0

b

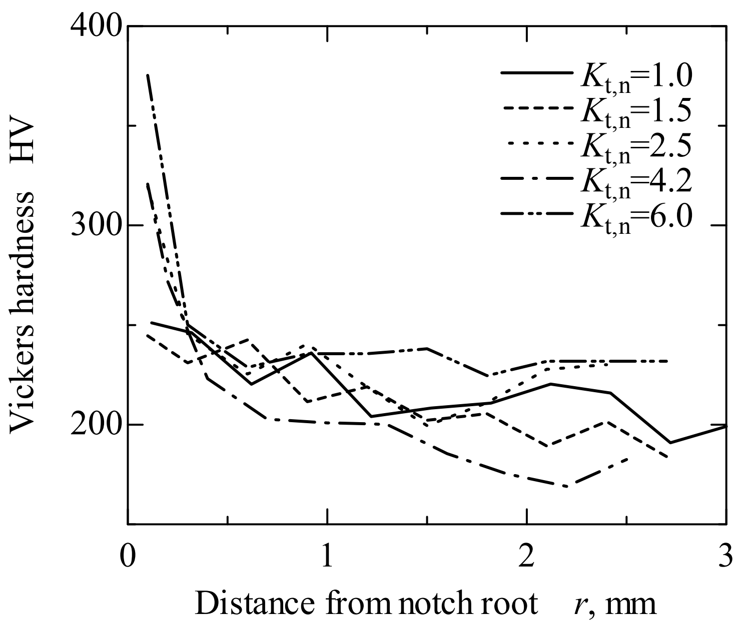

400
300
200
0
1
2
3
Vickers hardness HV
Distance from notch root r, mm
$K_{t,n}$=1.0
$K_{t,n}$=1.5
$K_{t,n}$=2.5
$K_{t,n}$=4.2
$K_{t,n}$=6.0

Fig. 7

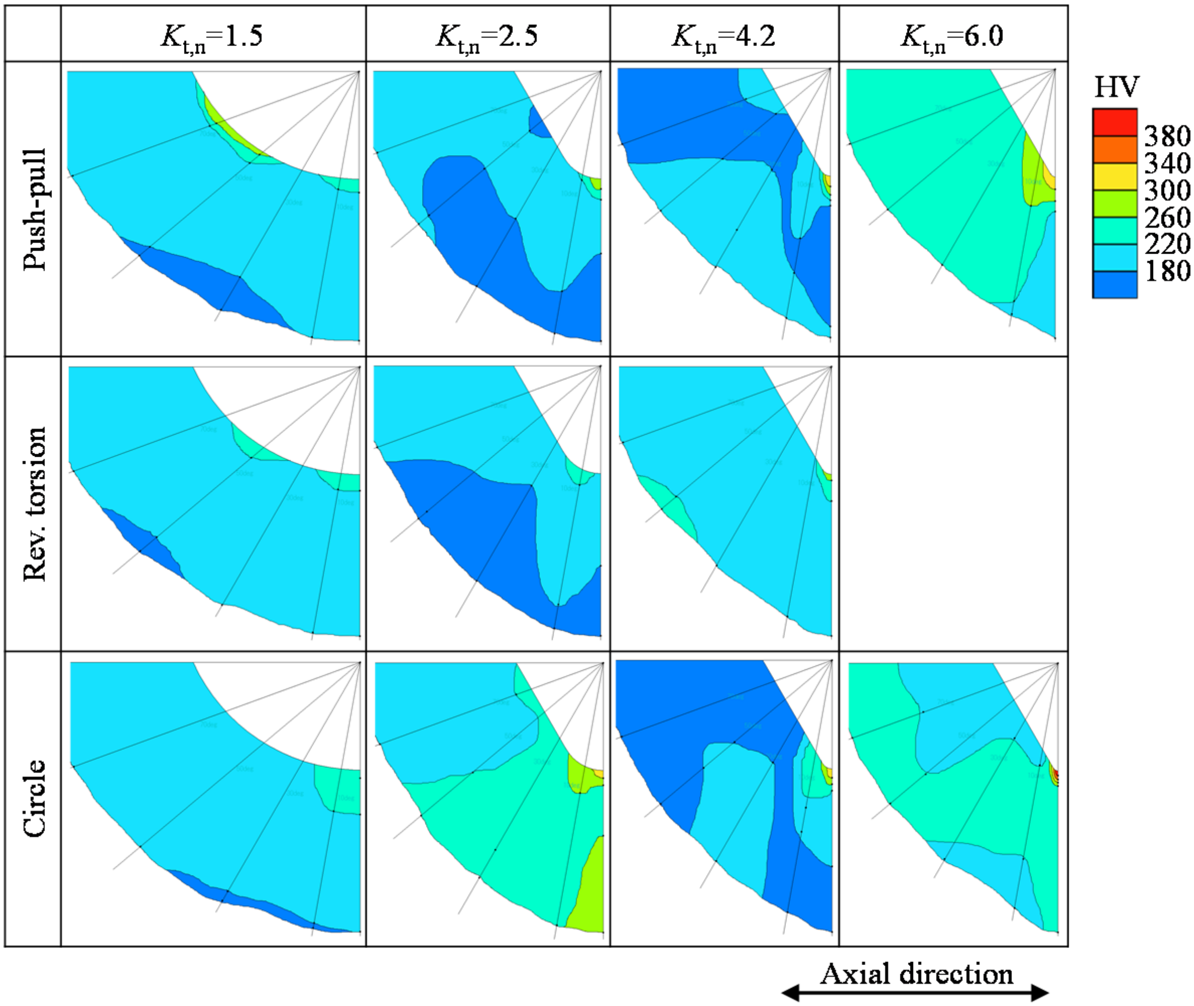

$K_{t,n}$=1.5
$K_{t,n}$=2.5
$K_{t,n}$=4.2
$K_{t,n}$=6.0
Push-pull
Rev. torsion
Circle
HV
380
340
300
260
220
180
Axial direction

Fig. 8

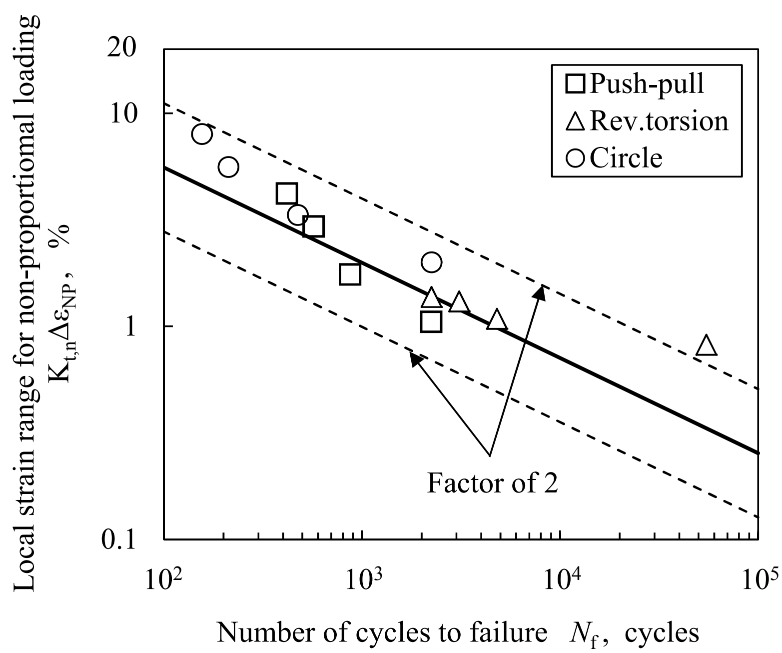

Local strain range for non-proportiomal loading
$K_{t,n}\Delta\varepsilon_{NP}$, %
20
10
1
0.1
10^2
10^3
10^4
10^5
Number of cycles to failure N_f, cycles
Push-pull
Rev.torsion
Circle
Factor of 2

Fig. 9

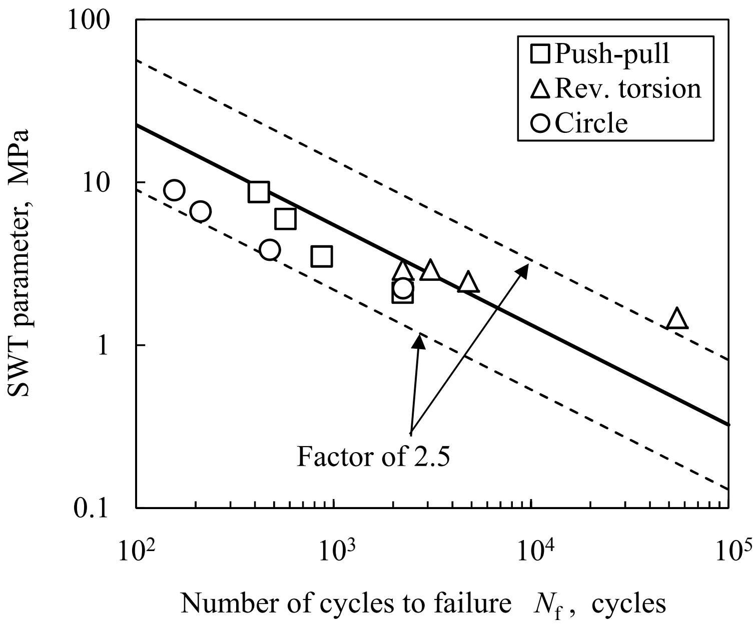
Push-pull
Rev. torsion
Circle
Factor of 2.5
SWT parameter, MPa
100
10
1
0.1
10^2
10^3
10^4
10^5
Number of cycles to failure N_f, cycles

Fig. 10

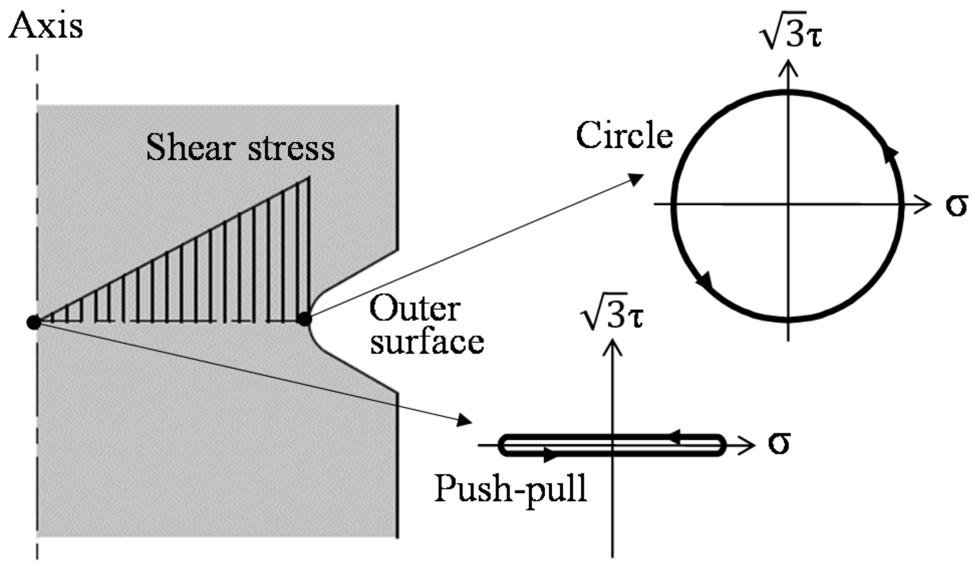

Axis
Shear stress
Outer
surface
$\sqrt{3}\tau$
Circle
σ
$\sqrt{3}\tau$
σ
Push-pull

Fig. 11

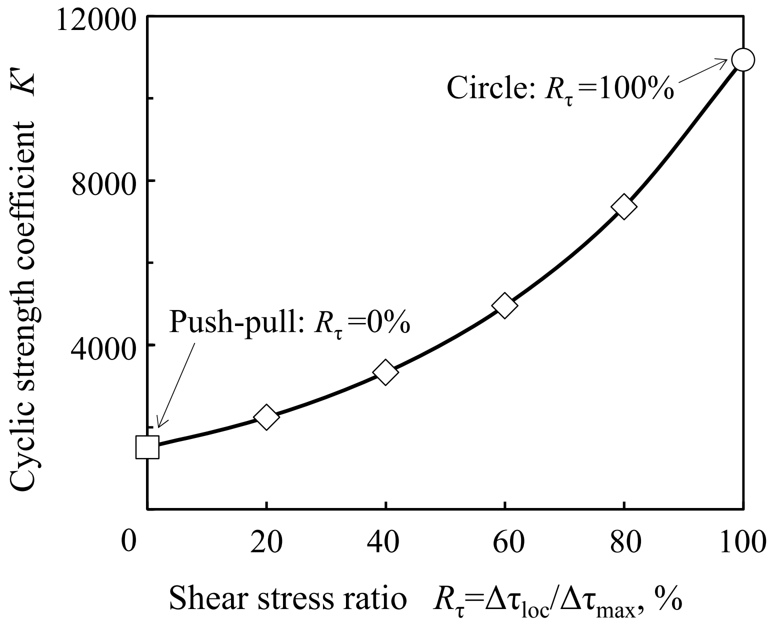

12000
8000
4000
Cyclic strength coefficient K'
Circle: R_τ=100%
Push-pull: R_τ=0%
0
20
40
60
80
100
Shear stress ratio $R_\tau=\Delta\tau_{loc}/\Delta\tau_{max}$, %

Fig. 12

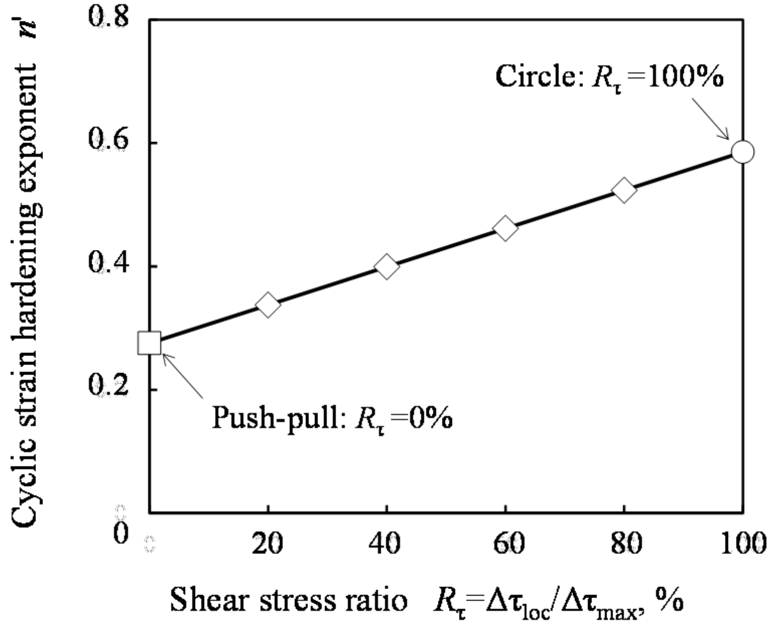

Cyclic strain hardening exponent n'
0.8
0.6
0.4
0.2
0
20
40
60
80
100
Circle: R_τ =100%
Push-pull: R_τ =0%
Shear stress ratio $R_\tau=\Delta\tau_{loc}/\Delta\tau_{max}$, %

Fig. 13

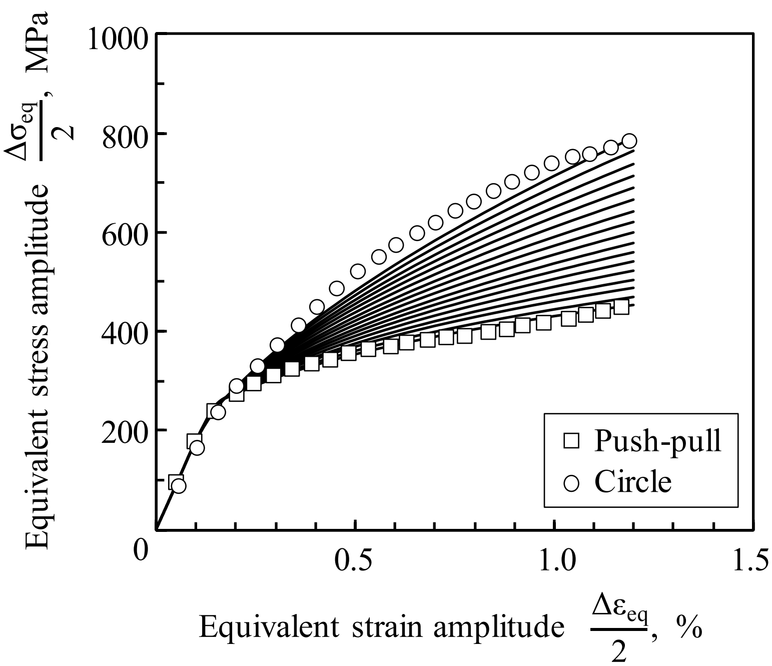

Equivalent stress amplitude $\frac{\Delta\sigma_{eq}}{2}$, MPa
1000
800
600
400
200
0
0.5
1.0
1.5
Equivalent strain amplitude $\frac{\Delta\varepsilon_{eq}}{2}$, %
Push-pull
Circle

Fig. 14

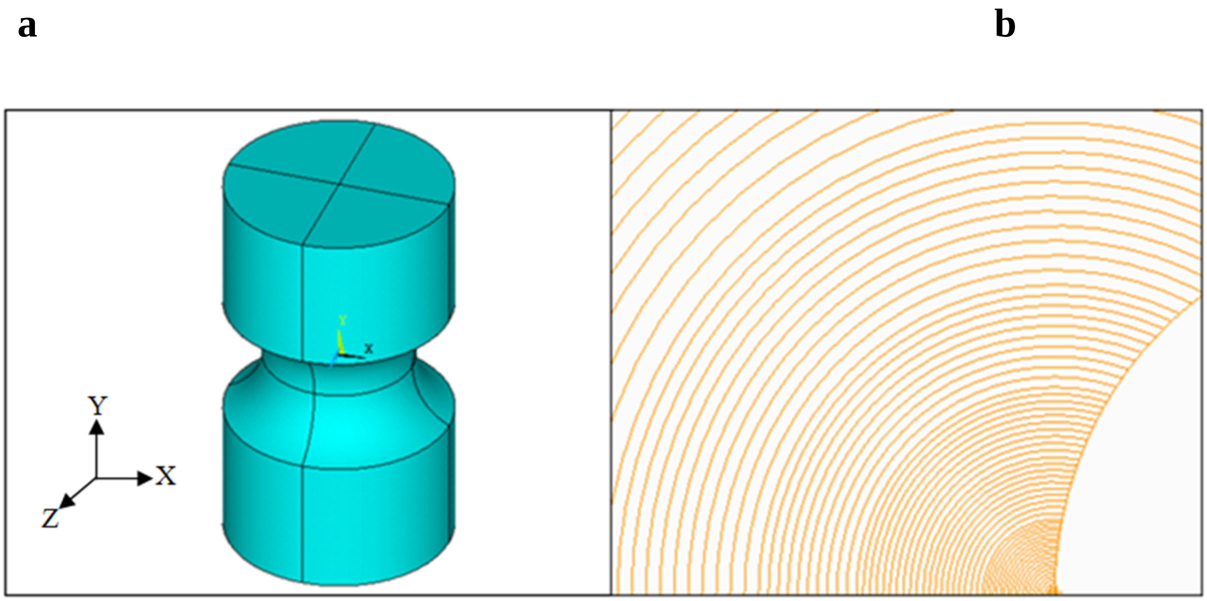

Fig. 15

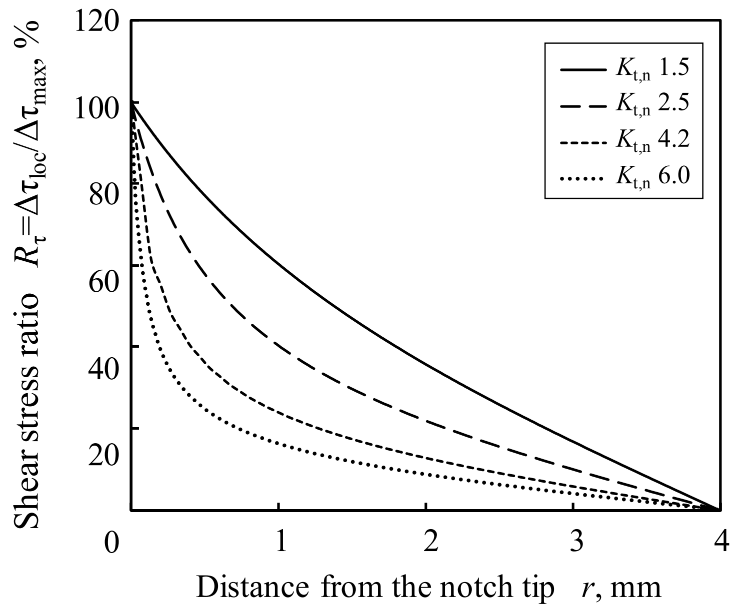

Shear stress ratio $R_\tau = \Delta\tau_{loc}/\Delta\tau_{max}$, %
120
100
80
60
40
20
0
1
2
3
4
Distance from the notch tip r, mm
$K_{t,n}$ 1.5
$K_{t,n}$ 2.5
$K_{t,n}$ 4.2
$K_{t,n}$ 6.0

Fig. 16

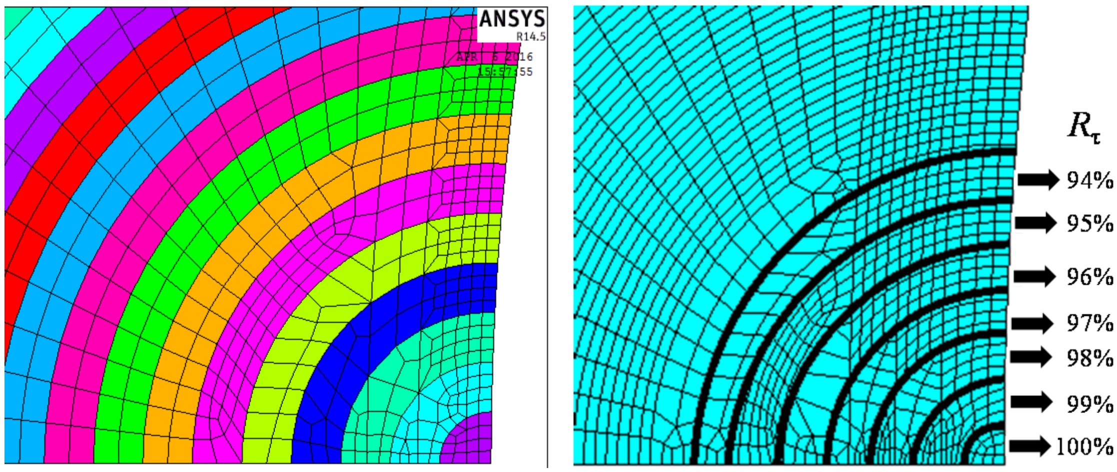

Fig. 17

a

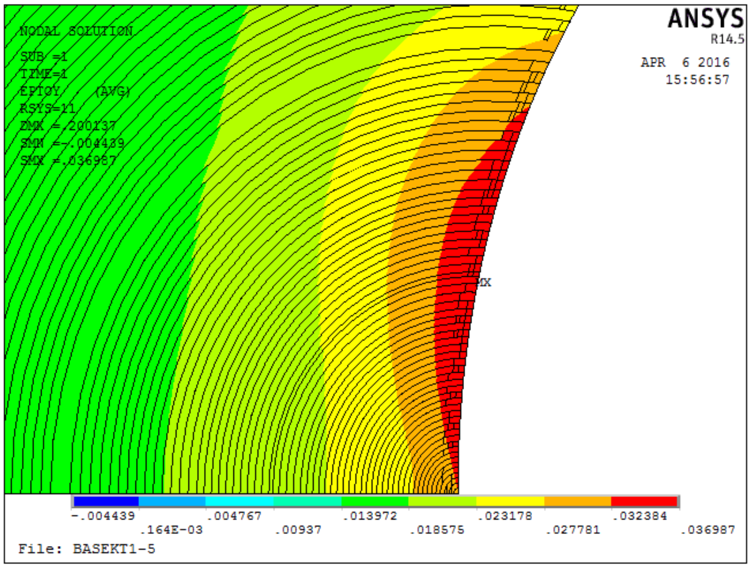
NODAL SOLUTION
SUB =1
TIME=1
EPTOY (AVG)
RSYS=11
DMX =.200137
SMN =-.004439
SMX =.036987
ANSYS
R14.5
APR 6 2016
15:56:57
MX
-.004439
.164E-03
.004767
.00937
.013972
.018575
.023178
.027781
.032384
.036987
File: BASEKT1-5

b

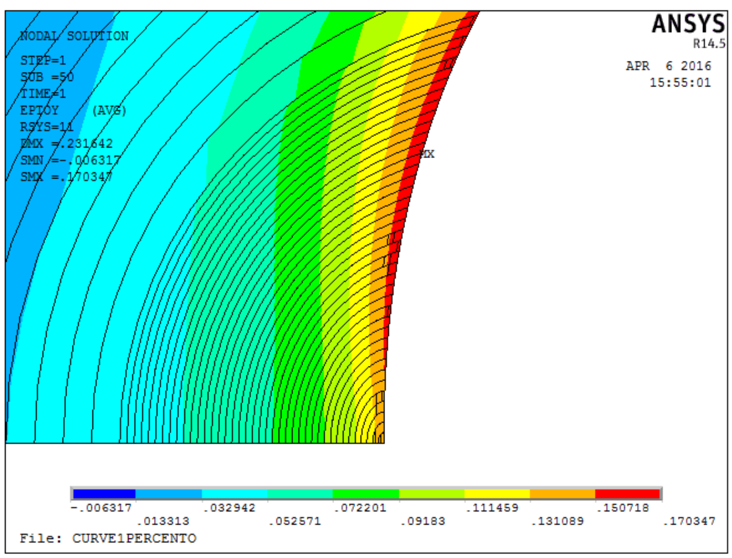
NODAL SOLUTION
STEP=1
SUB =50
TIME=1
EPTOY (AVG)
RSYS=11
DMX =.231642
SMN =-.006317
SMX =.170347
ANSYS
R14.5
APR 6 2016
15:55:01
MX
-.006317
.013313
.032942
.052571
.072201
.09183
.111459
.131089
.150718
.170347
File: CURVE1PERCENTO

Fig. 18

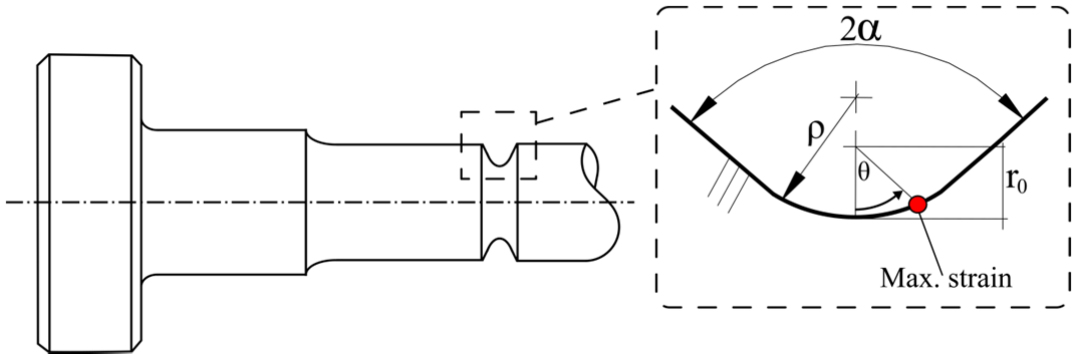

Fig. 19

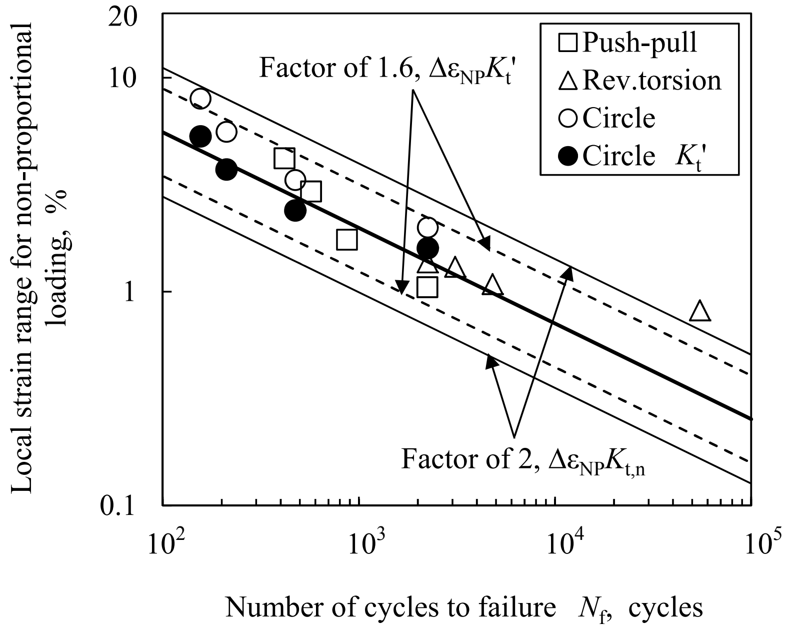
Push-pull
Rev.torsion
Circle
Circle K_t'
Factor of 1.6, $\Delta\varepsilon_{NP}K_t'$
Factor of 2, $\Delta\varepsilon_{NP}K_{t,n}$
Local strain range for non-proportional loading, %
Number of cycles to failure N_f, cycles
20
10
1
0.1
10^2
10^3
10^4
10^5

Fig. 20

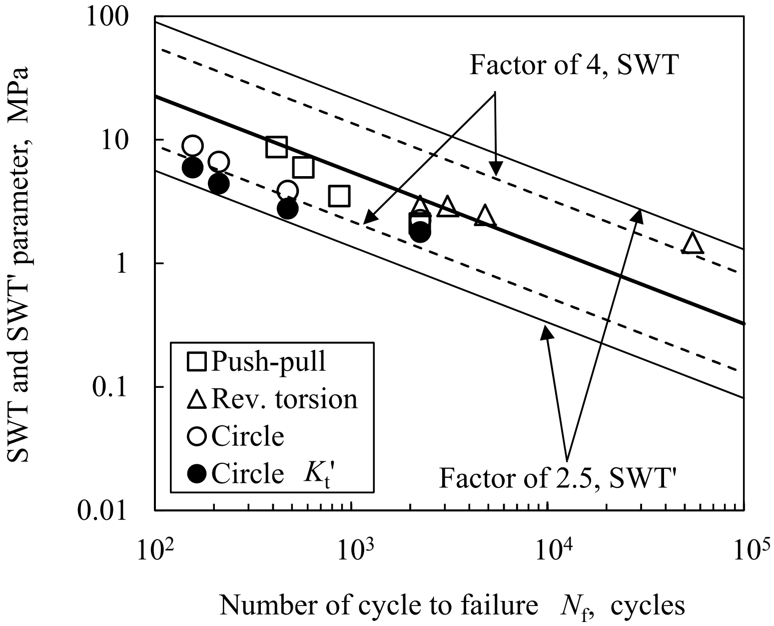

100
10
1
0.1
0.01
SWT and SWT' parameter, MPa
Factor of 4, SWT
Push-pull
Rev. torsion
Circle
Circle K_t'
Factor of 2.5, SWT'
10^2
10^3
10^4
10^5
Number of cycle to failure N_f, cycles